Structural Engineering and Mechanics, *Vol. 66, No. 5 (2018) 665-676*
DOI: https://doi.org/10.12989/sem.2018.66.5.665

An efficient partial mixed finite element model for static and free vibration analyses of FGM plates rested on two-parameter elastic foundations

M. Lezgy-Nazargah* and Z. Meshkani[a]

Faculty of Civil Engineering, Hakim Sabzevari University, Sabzevar 9617976487-397, Iran

(Received November 14, 2017, Revised February 24, 2018, Accepted February 27, 2018)

Abstract. In this study, a four-node quadrilateral partial mixed plate element with low degrees of freedom (dofs) is developed for static and free vibration analysis of functionally graded material (FGM) plates rested on Winkler-Pasternak elastic foundations. The formulation of the presented finite element model is based on a parametrized mixed variational principle which is developed recently by the first author. The presented finite element model considers the effects of shear deformations and normal flexibility of the FGM plates without using any shear correction factor. It also fulfills the boundary conditions of the transverse shear and normal stresses on the top and bottom surfaces of the plate. Beside these capabilities, the number of unknown field variables of the plate is only six. The presented partial mixed finite element model has been validated through comparison with the results of the three-dimensional (3D) theory of elasticity and the results obtained from the classical and high-order plate theories available in the open literature.

Keywords: FGM plate; thickness flexibility effects; partial mixed plate theory; finite element; elastic foundation

1. Introduction

FGMs plates are advanced hi-tech structures whose thermal and mechanical properties change continuously along the thickness direction. High resistance against high temperature gradients, smaller stress concentrations and attenuation of stress waves are some of the advantages of the FGMs against the traditional ones (Lezgy-Nazargah 2015a, Lezgy-Nazargah 2015b, Lezgy-Nazargah 2016a). Nowadays, FGM plate structures particularly those rested on elastic foundations have widespread applications in aerospace and mechanical engineering fields. Until now, various mathematical approaches are employed by researchers for the analysis FGM plates. These different numerical and analytical approaches can be investigated in the framework of two broad categories: approaches based on the 3D theory of elasticity, and approaches based the two-dimensional (2D) plate theories. These two classes are reviewed with more details in the two subsequent paragraphs.

Based on the 3D theory of elasticity, Huang *et al.* (2008) introduced an exact solution for simply supported FGM thick plates rested on Winkler–Pasternak foundations. They treated interactions between the elastic foundation and the FGM plate as boundary conditions. They solved the final system of the governing partial differential equations using the state space method. The extension of Huang *et al.* (2008) to free vibration analysis of simply supported FGM plates was done by Lu *et al.* (2009). By combining the differential quadrature method (DQM) with series solution approach, Malekzadeh (2009) studied 3D free vibration analysis of rectangular FGM plates with arbitrary boundary conditions rested on elastic foundations. Free vibration of FGM circular plates rested on the two-parameter elastic foundations with elastically restrained edges was studied by Shaban and Alipur (2011). They derived governing differential equations based on the first-order shear deformation theory (FSDT). They transformed the governing differential equations into algebraic recurrence equations by adopting a new semi-analytical differential transform method. A 3D Peano series solution was presented by Lezgy-Nazargah and Cheraghi (2017) for the bending analysis of imperfect layered FGM magneto-electro-elastic plates resting on two-parameter elastic foundations. In this reference, the state-space method is employed for solving the governing partial differential equations and the interfacial imperfection effects are taken into account using the concept of the generalized spring layer model. Based on the 3D theory of elasticity and using the DQM, Yas and Sobhani (2010) studied the free vibration of continuous grading fiber reinforced plates resting on Winkler-Pasternak elastic foundations.

Using a high-order shear and normal plate theory, Batra (2007) studied the free vibration of FGM incompressible elastic plates. In addition to the displacement components, Batra also assumed the hydrostatic pressure as independent variable. The plate theory of Batra is based on the principle of virtual work and it does not need the shear correction factor. Matsunga (2008) studied the free vibration and stability of FGM plates using a high-order plate theory. By employing various orders of expanded terms in the expression of the displacement components, Matsunga investigated the effects of high order deformations on the buckling loads and natural frequencies of the FGM plates.

*Corresponding author, Associate Professor
E-mail: m.lezgy@hsu.ac.ir
[a]M.Sc. Student

ISSN: 1225-4568 (Print), 1598-6217 (Online)

Vibration and buckling behavior of exponentially FGM sandwich plate resting on elastic foundations was investigated by Sobhy (2013). In this reference, it is assumed that the sandwich plate is made of a fully ceramic core layer with two metal/ceramic exponentially FGM coat. Sobhy deduced the governing equations by using the FSDT. An analytical solution was introduced by Baferani et al. (2011) for the free vibration of FGM plates rested on two-parameter elastic foundation. In this reference, which is restricted to the FGM plates with levy type of boundary conditions, the governing equations of motion are derived based on the third-order shear deformation plate theory (TSDT). By taking into account this assumption that the in-plane and transverse components of displacement field are composed of bending and shear parts, Thai and Choi (2012) introduced a refined shear deformation theory for vibration analysis of FGM plates rested on two-parameter elastic foundations. The refined plate theory of theses researchers contains only four unknown field variables and it gives a parabolic through-the-thickness distribution of the shear stresses without using any shear correction factor. By expanding the displacement components in the thickness direction using the Legendre polynomials, Sheikholeslami and Saidi (2013) studied the free vibration of simply supported rectangular FGM plates rested on two-parameter elastic foundation. They used a power law distribution for explaining through-the-thickness variations of the mechanical properties of the FGM plate. Based on a high-order hyperbolic shear deformation theory, Akavci (2014) studied the free vibration of FGM plates rested on two-parameter elastic foundations. In this work it is assumed that the transverse shear displacements vary as a hyperbolic function through the thickness of FGM plate. Using a trigonometric plate theory, Mantari and Soares (2014) obtained a Navier-type closed form solution for the bending analysis of single-layer and sandwich FGM plates. The trigonometric plate theory of these researchers has five unknown parameters and includes the thickness stretching effect. Mantari *et al*. (2014) investigated the static response of FGM plates using a tangential-exponential high-order shear deformation theory. The non-polynomial plate theory of this reference assumes a constant transverse displacement along the thickness of FGM plate and it does not require shear correction factor. Hadji *et al*. (2016) developed a new first shear deformation plate theory based on neutral surface position for the static and the free vibration analysis of FGM plates. Using a hyperbolic and parabolic shear and normal deformation theory, Daouadji and Adim (2017) studied the bending analysis of FGM sandwich plates. Using a sinusoidal shear deformation plate formulation which takes into account through-the-thickness deformations, Neves *et al*. (2011) investigated the static behavior of FGM plates. In this reference, the algebraic equations of motion are obtained by the Carrera's unified formulation (CUF), and further interpolated by radial basis functions. Based on the CUF, Brischetto and Carrera (2010) investigated the static response of FGM plates subjected to transverse mechanical loads. Note that the most of displacement-based and displacement-stress-based types of plate theories can be described precisely in the framework of CUF. In CUF, the principle of virtual displacements (PVD) is usually used for deriving the displacement-based plate theories while the displacement-stress-based plate theories are derived using the Reissner's mixed variational theorem (RMVT).

Due to coupling of the in-plane and transverse normal stresses, thickness flexibility effects should be considered for the accurate prediction of the responses of the thick FGM plates. In most of the available 2D displacement-based plate theories, the effects of the thickness flexibility of the FGM plate have been discarded. In limited works that the thickness flexibility effects are considered in the formulations, the boundary conditions of the transverse normal component of the stress tensor is not exactly fulfilled on the upper and lower planes of the FGM plate. Displacement-stress-based plate theories, which are mostly based on RMVT, can accurately capture the thickness flexibility effects in the FGM plates. The computational efficiency of the RMVT-based plate theories is dependent on the considered plate theory (i.e. the order of unknown expansion in the thickness direction). Due to considering of all transverse components of the stress tensor as primary unknown parameter, the number of unknown field variables of the mixed plate theories based on RMVT is very high. Recently, a new 2D partial mixed plate theory is introduced by Lezgy-Nazargah (2016b) for the analysis of thick plate structures. In this partial mixed plate theory which is based on the principle of parametrized mixed variational theorem, the transverse normal stress is considered as a primary variable in the formulations. The partial mixed plate theory of Lezgy-Nazargah (2016b) does not require the shear correction factor and fulfills the boundary conditions of the transverse shear and normal stresses on the top and bottom planes of the plate. Using this plate theory, one can predict through-the-thickness variations of transverse shear and normal stresses directly from the constitutive equations. The computational efficiency is the most interesting features of this plate theory. The number of unknown parameters of this plate theory is six which is one more than FSDT. In this study, the partial mixed plate theory of Lezgy-Nazargah (2016b) with some minor changes in its original kinematics is employed for studying the bending and free vibration responses of FGM plates rested on two-parameter elastic foundations. It is assumed that the material properties of the plate vary along the thickness direction according to the volume fraction of constituents. Both power-law and exponent function are used for defining the volume fraction constituents of the FGM plate. A quadrilateral four-node plate element with 21 dofs per node is employed for numerical solving of the governing equations of motion. In the employed finite element, the deflection (transverse displacement) of the FGM plate is interpolated using the full Hermitian shape functions. Lagrange shape functions are employed for interpolating of the other field variables of the FGM plate.

The paper is outlined as follows: the main mathematical formulations of the new four-node quadrilateral plate element are fully described in Sections 2 and 3. Numerical results which involve various bending and free vibration tests are subsequently presented in Section 4. Conclusion

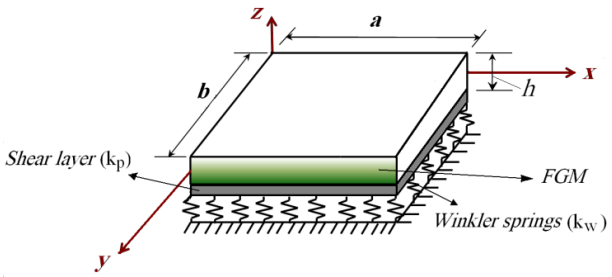

Fig. 1 The FGM plate and the considered Cartesian coordinate system

and recommendations for future researches are given in Section 5.

2. Theoretical formulation

As shown in Fig. 1, the considered FGM plate of the present study is rested on a Winkler-Pasternak type elastic foundation and it occupies the domain $V=\Omega\times\left[-h/2\le z\le h/2\right]$ in the Cartesian coordinate system (x,y,z). Ω is an arbitrary surface in the (x,y) plane which is located at the mid-plane (z=0) of the FGM plate. k_w and k_p denote the stiffness of the Winkler and shear springs, respectively.

2.1 Constitutive equations

It is assumed that the mechanical properties of the plate vary continuously through the thick direction according to the one of the following distributions:

Power-law distribution

$$P(z)=P_{bottom}+(P_{top}-P_{bottom})(\frac{1}{2}+\frac{z}{h})^n \tag{1.a}$$

Exponent-law distribution

$$P(z)=P_{bottom}e^{n(1/2+z/h)} \tag{1.b}$$

where P represents the effective material properties (e.g., mass density (ρ), Young's modulus (E), ….) and n is the material gradient index. Due to very small effects of the variations of Poisson's ratio (ν) on the response of FGM plates (Yang *et al.* 2005, Kitipornchai *et al.* 2006), it is assumed to be a constant value through the plate thickness. Using the matrix notations, the 3D constitutive equations for the FGM plate can be expressed as

$$\begin{Bmatrix}\boldsymbol{\sigma}_p\\ \boldsymbol{\sigma}_z\end{Bmatrix}=\begin{bmatrix}\boldsymbol{D}_{pp} & \boldsymbol{D}_{pz}\\ \boldsymbol{D}_{pz}^T & \boldsymbol{D}_{zz}\end{bmatrix}\times\begin{Bmatrix}\boldsymbol{\varepsilon}_p\\ \boldsymbol{\varepsilon}_z\end{Bmatrix} \tag{2}$$

where

$\boldsymbol{\varepsilon}_p=\{\varepsilon_{11}\quad\varepsilon_{22}\quad 2\varepsilon_{12}\quad 2\varepsilon_{23}\quad 2\varepsilon_{13}\}^T$,

$\boldsymbol{\sigma}_p=\{\sigma_{11}\quad\sigma_{22}\quad\sigma_{12}\quad\sigma_{23}\quad\sigma_{13}\}^T$,

$\boldsymbol{\varepsilon}_z=\{\varepsilon_{33}\}$, $\boldsymbol{\sigma}_z=\{\sigma_{33}\}$

and σ_{ij} and ε_{ij} are the stress and strain components, respectively. $\boldsymbol{D}_{pp}$, $\boldsymbol{D}_{pz}$ and $\boldsymbol{D}_{zz}$ denote the elastic coefficients matrices whose explicit expressions are given in Appendix A. Since the transverse normal stress component (σ_{33}) of the FGM plate is taken as a priori variables, the constitutive relations (2) should be rewritten as follows

$$\begin{Bmatrix}\boldsymbol{\sigma}_p\\ \boldsymbol{\varepsilon}_z\end{Bmatrix}=\begin{bmatrix}\hat{\boldsymbol{D}}_{pp} & \hat{\boldsymbol{D}}_{pz}\\ \hat{\boldsymbol{D}}_{pz}^T & \hat{\boldsymbol{D}}_{zz}\end{bmatrix}\times\begin{Bmatrix}\boldsymbol{\varepsilon}_p\\ \boldsymbol{\sigma}_z\end{Bmatrix} \tag{3}$$

where

$$\begin{aligned}&\hat{D}_{pp}=D_{pp}-D_{pz}(D_{zz})^{-1}D_{zp},\ \hat{D}_{pz}=D_{pz}(D_{zz})^{-1}\\&\hat{D}_{zp}=-(D_{zz})^{-1}D_{zp},\ \hat{D}_{zz}=(D_{zz})^{-1}\end{aligned} \tag{4}$$

2.2 Kinematics

The following particular relations are used for representing the total displacement components of the FGM plate

$$\begin{aligned}U(x,y,z)=u(x,y)-z\frac{\partial w_1}{\partial x}-f(z)\frac{\partial w_2}{\partial x}-\frac{z^2}{2}\frac{\partial w_3}{\partial x}\\+z\frac{T_x^+-T_x^-}{2D_{55}}+\frac{z^2}{2hD_{55}}(T_x^++T_x^-)\end{aligned} \tag{5.a}$$

$$\begin{aligned}V(x,y,z)=v(x,y)-z\frac{\partial w_1}{\partial y}-f(z)\frac{\partial w_2}{\partial y}-\frac{z^2}{2}\frac{\partial w_3}{\partial y}\\+z\frac{T_y^+-T_y^-}{2D_{44}}+\frac{z^2}{2hD_{44}}(T_y^++T_y^-)\end{aligned} \tag{5.b}$$

$$W(x,y,z)=w_1(x,y)+w_2(x,y)+z\,w_3(x,y) \tag{5.c}$$

where $u(x,y)$ and $v(x,y)$ denote the in-plane displacements of a point on the reference surface of plate. T_x^+, T_x^-, and T_y^+, T_y^- represent the tangential components of force vectors applied to the external upper and lower surfaces of the FGM plate. $w_1(x,y)$ and $w_2(x,y)$ denotes the bending and shearing part of the transverse displacement component, respectively. $f(z)=z-ze^{-2(z/h)^2}$ and $w_3(x,y)$ is an unknown parameter function.

The displacement field given in Eq. (5) can be expressed in the following matrix form

$$\boldsymbol{u}=\boldsymbol{A}_u\boldsymbol{u}_u \tag{6}$$

where $\boldsymbol{u}=\begin{bmatrix}U & V & W\end{bmatrix}^T$,

$\boldsymbol{u}_u=\begin{bmatrix}u & v & w_1 & w_2 & w_3 & T_x^+ & T_x^- & T_y^+ & T_y^-\end{bmatrix}^T$ and

$$\boldsymbol{A}_u=\begin{bmatrix} 1 & 0 & -z\dfrac{\partial}{\partial x} & -f(z)\dfrac{\partial}{\partial x} & -\dfrac{z^2}{2}\dfrac{\partial}{\partial x} \\ 0 & 1 & -z\dfrac{\partial}{\partial y} & -f(z)\dfrac{\partial}{\partial y} & -\dfrac{z^2}{2}\dfrac{\partial}{\partial y} \\ 0 & 0 & 1 & 1 & z \\ & & & & \end{bmatrix}$$

$$\begin{matrix} (\dfrac{z}{2D_{55}}+\dfrac{z^2}{2hD_{55}}) & (-\dfrac{z}{2D_{55}}+\dfrac{z^2}{2hD_{55}}) \\ 0 & 0 \\ 0 & 0 \\ 0 & 0 \\ (\dfrac{z}{2D_{44}}+\dfrac{z^2}{2hD_{44}}) & (-\dfrac{z}{2D_{44}}+\dfrac{z^2}{2hD_{44}}) \\ 0 & 0 \end{matrix} \quad (7)$$

2.3 Transverse normal stress assumptions

In order to fulfill the boundary conditions of the transverse normal stress on the top and bottom surface of the FGM plate, it is assumed as a priori unknown variable. Variations of the transverse normal stress through the thickness of the FGM plate are approximated using the following second-order expansion

$$\begin{aligned}\sigma_{zz}^{*}(x,y,z)=L_1(z)T_z^{-}(x,y)+L_2(z)\varphi(x,y)\\ +L_3(z)T_z^{+}(x,y)\end{aligned} \quad (8)$$

In the above equation $\varphi(x,y)$ is an unknown stress field variable. $T_z^{+}(x,y)$ and $T_z^{-}(x,y)$ are the normal component of traction vectors applied on the external top and bottom surfaces of the FGM plate, respectively. $L_i(z)$ $(i=1,2,3)$ denote the quadratic Lagrange interpolation functions (see Appendix A).

The above equation can be rewritten in the matrix form as below

$$\boldsymbol{\sigma}=\boldsymbol{A}_\sigma\boldsymbol{u}_\sigma \quad (9)$$

where $\boldsymbol{\sigma}=\left[\bar{\sigma}_{zz}\right]$, $\boldsymbol{u}_\sigma=\left[T_z^{-} \quad \varphi \quad T_z^{+}\right]^T$, and $\boldsymbol{A}_\sigma=\left[L_1(z) \quad L_2(z) \quad L_3(z)\right]$.

3. Finite element formulation

3.1 Approximations of displacement and stress fields

Based on the displacement and transverse normal stress fields introduced in sections 2.3 and 2.4, the present plate formulation contains totally 12 field variables u, v, w_1, w_2, w_3, φ, T_z^{-}, T_z^{-}, T_x^{+}, T_x^{-}, T_y^{+} and T_y^{-}. However, T_z^{-}, T_z^{-}, T_x^{+}, T_x^{-}, T_y^{+}, T_y^{-} are the prescribed shear and normal tractions on the upper and lower planes of the FGM plate. Since the values of these aforementioned six parameters are known before analysis, the present partial mixed plate formulation has finally six unknown parameters u, v, w_1, w_2, w_3 and φ. A four-node quadrilateral element is constructed for the static bending and free vibration analyses of the FGM plates. The geometry of the element is approximated using the bi-linear Lagrangian interpolation functions. Full compatible Hermitian shape functions are used for interpolating the in-plane variations of the unknown parameters of the transverse displacement component (w_1, w_2, w_3) while bi-linear Lagrange shape functions with C^0-type continuity are employed for interpolating of the other unknown field variables of the FGM plate. Thus, the unknown functions of the displacement and stress fields can be expressed in terms of the corresponding nodal variables as below

$$\boldsymbol{u}_u=\boldsymbol{N}_u\hat{\boldsymbol{u}}_u^e \quad (10.a)$$

$$\boldsymbol{u}_\sigma=\boldsymbol{N}_\sigma\hat{\boldsymbol{u}}_\sigma^e \quad (10.b)$$

where $\hat{\boldsymbol{u}}_u^e$ and $\hat{\boldsymbol{u}}_\sigma^e$ are the vector of the nodal values of the displacement and stress fields, respectively. $\boldsymbol{N}_u$ and $\boldsymbol{N}_\sigma$ are matrices which contain the interpolation functions. The expression for $\boldsymbol{N}_u$ and $\boldsymbol{N}_\sigma$ are not cited here for the sake of brevity. The considered four-node quadrilateral element has the following 21 dofs per node

$$\begin{matrix} u & v & w_1 & (w_1)_{,x} & (w_1)_{,y} & (w_1)_{,xy} & w_2 \\ (w_2)_{,x} & (w_2)_{,y} & (w_2)_{,xy} & w_3 & (w_3)_{,x} & (w_3)_{,y} & (w_3)_{,xy} \\ \varphi & T_x^{+} & T_x^{-} & T_y^{+} & T_y^{-} & T_z^{+} & T_z^{-} \end{matrix} \quad (11)$$

For more details about the finite element model, the interested readers can refer to Lezgy-Nazargah (2016b).

Using Eqs. (10-a) and (10-b), the displacement and transverse normal stress of the FGM plate can be finally rewritten in terms of the nodal variables of the element as follows

$$\boldsymbol{u}=A_u\boldsymbol{u}_u=A_uN_u\hat{\boldsymbol{u}}_u^e=X_u\hat{\boldsymbol{u}}_u^e \quad (12.a)$$

$$\boldsymbol{\sigma}=A_\sigma\boldsymbol{u}_\sigma=A_\sigma N_\sigma\hat{\boldsymbol{u}}_\sigma^e=X_\sigma\hat{\boldsymbol{u}}_\sigma^e \quad (12.b)$$

Using well-known strain-displacement relations with considering Eqs. (12-a) and (12-b), the strain vectors $\boldsymbol{\varepsilon}_p$ and $\boldsymbol{\varepsilon}_z$ can also be expressed in terms of the nodal variables of the element

$$\boldsymbol{\varepsilon}_p=\boldsymbol{C}_p\boldsymbol{u}=\boldsymbol{C}_p\boldsymbol{X}_u\boldsymbol{u}_u^e \quad (13.a)$$

$$\boldsymbol{\varepsilon}_z=\boldsymbol{C}_z\boldsymbol{u}=\boldsymbol{C}_z\boldsymbol{X}_u\boldsymbol{u}_u^e \quad (13.b)$$

in which the differential matrices are

$$\boldsymbol{C}_p=\begin{bmatrix}\frac{\partial}{\partial x} & 0 & 0\\ 0 & \frac{\partial}{\partial y} & 0\\ \frac{\partial}{\partial y} & \frac{\partial}{\partial x} & 0\\ 0 & \frac{\partial}{\partial z} & \frac{\partial}{\partial y}\\ \frac{\partial}{\partial z} & 0 & \frac{\partial}{\partial x}\end{bmatrix},\quad \boldsymbol{C}_z=\begin{bmatrix}0 & 0 & \frac{\partial}{\partial z}\end{bmatrix} \tag{14}$$

3.2 Governing equations

The discretized form of the governing equations of motion is derived in this section. The element mass and stiffness matrices as well as the vector of external loadings of the FGM plate are obtained via the parametrized mixed variational theorem of Lezgy-Nazargah (2016b). According to this variational principle, the total potential energy of an FGM plate with volume Ω and regular boundary surfaces S can be written as

$$\begin{aligned}\Pi_p=&\frac{1}{2}\int_{\Omega}\Big(\boldsymbol{\varepsilon}_p^T\boldsymbol{D}_{pp}\boldsymbol{\varepsilon}_p+\beta\boldsymbol{\varepsilon}_p^T\boldsymbol{D}_{pz}\boldsymbol{\varepsilon}_z\\ &+\beta\boldsymbol{\varepsilon}_z^T\boldsymbol{D}_{zp}\boldsymbol{\varepsilon}_p+\beta\boldsymbol{\varepsilon}_z^T\boldsymbol{D}_{zz}\boldsymbol{\varepsilon}_z\Big)d\Omega\\ &+\frac{1}{2}\int_{\Omega}(1-\beta)\Big(-\boldsymbol{\sigma}_z^{*T}\hat{\boldsymbol{D}}_{zz}^T\boldsymbol{\sigma}_z^*+2\boldsymbol{\sigma}_z^{*T}\hat{\boldsymbol{D}}_{zz}\boldsymbol{D}_{zp}\boldsymbol{\varepsilon}_P\\ &+2\boldsymbol{\sigma}_z^{*T}\boldsymbol{\varepsilon}_z+\boldsymbol{\varepsilon}_p^T\hat{\boldsymbol{D}}_{zp}^T\boldsymbol{D}_{zp}\boldsymbol{\varepsilon}_P\Big)d\Omega\\ &+\int_S\boldsymbol{u}^T\boldsymbol{P}\,dS+\int_{\Omega}\boldsymbol{u}^T\boldsymbol{p}\,d\Omega\end{aligned} \tag{15}$$

where $\boldsymbol{p}$ and $\boldsymbol{P}$ are the vector of body and surface forces, respectively. β is an arbitrary parameter function which is called the splitting factor. As demonstrated in Lezgy-Nazargah (2016b), the appearance of the splitting factor in the variational formulation has some numerical advantages. By selecting an appropriate splitting factor, one can adjust the shares of the potential and complementary energy and consequently increase the accuracy of the numerical results. In order to avoid the complexity of the formulation, the values of splitting factor in this study is assumed to be β=0. In this case, the functional of Eq. (15) reduces into a partial mixed form of the Reissner's variational theorem. The dissection about the optimal value of β is out of the scope of the present paper and will be addressed in future researches. The total strain energy expressions associated with the Winkler-Pasternak foundation can be written as (Buczkowski and Torbacki 2001)

$$\Pi_F=\frac{1}{2}\int_S\Big(k_w\boldsymbol{u}^T\boldsymbol{I}_w^T\boldsymbol{I}_w\boldsymbol{u}+k_p\boldsymbol{u}^T\boldsymbol{C}_w^T\boldsymbol{C}_w\boldsymbol{u}\Big)dS \tag{16}$$

where

$$\boldsymbol{I}_w=\begin{bmatrix}0&0&0\\0&0&0\\0&0&1\end{bmatrix},\quad \boldsymbol{C}_w=\begin{bmatrix}0&0&\partial/\partial x\\0&0&\partial/\partial y\end{bmatrix} \tag{17}$$

By substituting Eqs. (3), (11) and (13) into the above energy expressions (Eqs. (15)-(16)), the following governing equations of motion will be obtained from the Hamilton's principle

$$\boldsymbol{M}\,\ddot{\boldsymbol{\alpha}}(t)+\boldsymbol{K}\,\boldsymbol{\alpha}(t)=\boldsymbol{F}(t) \tag{18}$$

where $\boldsymbol{M}$ and $\boldsymbol{K}$ denote the total mass and stiffness matrices, respectively. $\boldsymbol{\alpha}$ is the total nodal variables vector in global coordinates while $\boldsymbol{F}$ is the total load vector. The aforementioned matrices are obtained from assembling the corresponding elementary matrices as below

$$\boldsymbol{K}=\sum_e\boldsymbol{K}^e,\ \boldsymbol{M}=\sum_e\boldsymbol{M}^e,\ \boldsymbol{F}=\sum_e\boldsymbol{F}^e,\ \boldsymbol{\alpha}=\sum_e\boldsymbol{\alpha}^e \tag{19}$$

The elementary mass matrix $\boldsymbol{M}^e$ can be written as

$$\boldsymbol{M}^e=\begin{bmatrix}\boldsymbol{M}_{uu}^e & \boldsymbol{0}\\ \boldsymbol{0} & \boldsymbol{0}\end{bmatrix} \tag{20}$$

where

$$\boldsymbol{M}_{uu}^e=\int_{\Omega^e}[\boldsymbol{X}_u^T\rho\boldsymbol{X}_u\ ]d\Omega \tag{21}$$

The elementary stiffness matrix $\boldsymbol{K}^e$ can be also written as

$$\boldsymbol{K}^e=\begin{bmatrix}\boldsymbol{K}_{uu}^e & \boldsymbol{K}_{\sigma u}^{eT}\\ \boldsymbol{K}_{\sigma u}^e & \boldsymbol{K}_{\sigma\sigma}^e\end{bmatrix} \tag{22}$$

where

$$\begin{aligned}\boldsymbol{K}_{uu}^e=&\int_{\Omega^e}[\boldsymbol{X}_u^T\boldsymbol{C}_p^T\boldsymbol{D}_{pp}\boldsymbol{C}_p\boldsymbol{X}_u+\boldsymbol{X}_u^T\boldsymbol{C}_p^T\hat{\boldsymbol{D}}_{zp}^T\boldsymbol{D}_{zp}\boldsymbol{C}_p\boldsymbol{X}_u\ ]d\Omega\\ &+\int_{S^e}\Big(k_w\boldsymbol{X}_u^T\boldsymbol{I}_w^T\boldsymbol{I}_w\boldsymbol{X}_u+k_p\boldsymbol{X}_u^T\boldsymbol{C}_w^T\boldsymbol{C}_w\boldsymbol{X}_u\Big)dS\\ \boldsymbol{K}_{\sigma u}^e=&\int_{\Omega^e}[\boldsymbol{X}_\sigma^T\hat{\boldsymbol{D}}_{zz}\boldsymbol{D}_{zp}\boldsymbol{C}_p\boldsymbol{X}_u+\boldsymbol{X}_\sigma^T\boldsymbol{C}_z\boldsymbol{X}_u]d\Omega\\ \boldsymbol{K}_{\sigma\sigma}^e=&\int_{\Omega^e}[-\boldsymbol{X}_\sigma^T\hat{\boldsymbol{D}}_{zz}^T\boldsymbol{X}_\sigma]d\Omega\end{aligned} \tag{23}$$

The elementary vector of dofs $\boldsymbol{\alpha}^e$ can be written as

$$\boldsymbol{\alpha}^e=\begin{Bmatrix}\hat{\boldsymbol{\alpha}}_u\\ \hat{\boldsymbol{\alpha}}_\sigma\end{Bmatrix} \tag{24}$$

where $\hat{\boldsymbol{\alpha}}_u$ and $\hat{\boldsymbol{\alpha}}_\sigma$ are the elementary nodal variables of the displacement and the transverse normal stress fields, respectively. Finally, the elementary load vector $\boldsymbol{F}^e$ may be written a

$$\boldsymbol{F}^e=\begin{bmatrix}\boldsymbol{F}_u^e\\ \boldsymbol{F}_\sigma^e\end{bmatrix}=\begin{bmatrix}\int_{S^e}\boldsymbol{X}_u^T\boldsymbol{P}\,dS+\int_{\Omega^e}\boldsymbol{X}_u^T\boldsymbol{p}\,d\Omega\\ \boldsymbol{0}\end{bmatrix} \tag{25}$$

4. Numerical results

In this section, static bending and free vibration analyses of FGM plates rested on Winkler-Pasternak elastic foundations are carried out using the proposed finite element model. For the validation purposes, the present results are compared with both the classical and recent advanced plate theories. Some comparisons are also made with the solutions of the 3D theory of elasticity.

4.1 Example 1

A square FGM plate (a=b=1) consisting of aluminum (bottom plane) and alumina (top plane) is considered. The considered graded plate is simply supported and the bi-sinusoidal transverse load $T_z^{+} = q_0 \sin\frac{\pi x}{a}\sin\frac{\pi y}{b}$ is applied on its top surface ($z = h/2$). The thickness ratio of the considered FGM plate is a/h=0.1. It is assumed that the Young's modulus varies along the thickness direction of plate according to the following relation

$$E(z) = E_m + (E_c - E_m)\left(\frac{1}{2} + \frac{z}{h}\right)^n$$

where $E_c = 380\,\text{GPa}$ and $E_m = 70\,\text{GPa}$ denote the Young's modulus of alumina (ceramic) and aluminum (metal), respectively. n is the material gradient index of the graded plate which takes positive values. The Poisson's ratio is assumed constant (ν=0.3) in both metal and ceramic. Note that the following non-dimensional quantities used in this example

$$\bar{w} = \frac{10h^3E_c}{a^4q_0}\times w\left(\frac{a}{2},\frac{b}{2}\right),\quad \bar{u} = \frac{100h^3E_c}{a^4q_0}\times u\left(\frac{a}{2},\frac{b}{2},-\frac{h}{4}\right)$$

$$\bar{v} = \frac{100h^3E_c}{a^4q_0}\times v\left(\frac{a}{2},\frac{b}{2},-\frac{h}{6}\right),\quad \bar{\sigma}_{xy} = \frac{h}{aq_0}\times\sigma_{xy}\left(0,0,-\frac{h}{3}\right)$$

$$\bar{\sigma}_{xx} = \frac{h}{aq_0}\times\sigma_{xx}\left(\frac{a}{2},\frac{b}{2},\frac{h}{2}\right),\quad \bar{\sigma}_{yy} = \frac{h}{aq_0}\times\sigma_{yy}\left(\frac{a}{2},\frac{b}{2},\frac{h}{3}\right)$$

$$\bar{\sigma}_{yz} = \frac{h}{aq_0}\times\sigma_{yz}\left(\frac{a}{2},0,\frac{h}{6}\right),\quad \bar{\sigma}_{xz} = \frac{h}{aq_0}\times\sigma_{xz}\left(0,\frac{b}{2},0\right)$$

$$\bar{\sigma}_{zz} = \frac{1}{q_0}\times\sigma_{zz}\left(\frac{a}{2},\frac{b}{2},\frac{h}{2}\right)$$

4.1.1 Mesh convergence study

The sensitivity of the proposed partial mixed finite element model with respect to the number of elements is investigated in this subsection. To this aim, the considered simply supported FGM plate is analyzed using the present finite element model with 2×2, 4×4 and 8×8 elements. The obtained numerical results are given in Table 1 for two material gradient indexes n=1, 10. It can be seen that the convergence velocity of the present partial mixed finite element model is high. Deflection of the FGM plate is insensitive to the number of elements and only 4×4 elements are enough for a bending test. Regardless of the values of the material gradient index, a mesh with 8×8 elements leads to the converged results for both deflection and stress components. The obtained numerical results of Table 1 shows that a mesh with 8×8 elements is sufficient for carrying out a static bending test using the present partial mixed finite element model. Based on the results of the convergence mesh study, all the subsequent numerical results are obtained using a mesh with 8×8 elements.

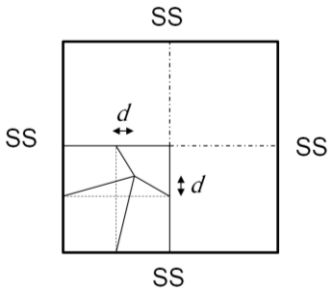

Fig. 2 Mesh sensitivity test: simply supported FGM plate under transverse bi-sinusoidal load-(n=10)

Table 1 Results of the convergence mesh study for the simply supported FGM plates under bi-sinusoidal transverse load

n	Mesh (number of dofs)	$\bar{w}$	$\bar{\sigma}_{xx}$	$\bar{\sigma}_{yz}$	$\bar{\sigma}_{xz}$	$\bar{\sigma}_{xy}$	$\bar{\sigma}_{zz}$
1	2×2 (189)	0.5833	3.8051	0.2610	0.2059	0.5663	1.0000
	4×4 (525)	0.5832	3.3438	0.2604	0.2502	0.6043	1.0000
	8×8 (1701)	0.5831	3.1291	0.2601	0.2503	0.6045	1.0000
	16×16 (6069)	0.5831	3.1291	0.2600	0.2503	0.6045	1.0000
10	2×2 (189)	0.9949	9.2853	0.2125	0.2362	0.6921	1.0000
	4×4 (525)	1.0012	5.1553	0.2064	0.2273	0.5787	1.0000
	8×8 (1701)	1.0009	5.1410	0.2032	0.2262	0.5730	1.0000
	16×16 (6069)	1.0009	5.1410	0.2032	0.2261	0.5730	1.0000

Table 2 Results of the mesh distortion test

	d			
	0	0.04	0.08	0.12
$\bar{w}$	1.0012	1.0252	1.0022	0.9179

4.1.2 Mesh distortion test

In this subsection, the robustness of the present partial mixed finite element model with respect to the distortion of meshes is investigated. The considered FGM plate is analyzed using the present finite element formulation with both regular (d=0) and distorted (d>0) meshes. These employed meshes as well as the distortion index d are shown in Fig. 2. For different values of the distortion index d, the non-dimensional transverse deflection ($\bar{w}$) of the FGM plate with material gradient parameter n=10 is given in Table 2. As shown in this table, the discrepancy between the results obtained from a regular mesh (d=0) with those obtained from a highly distorted mesh (d=0.12) is about 9%. These numerical results prove that the present partial mixed finite element model is not sensitive to the mesh distortion. Due to using the full compatible Hermitian shape functions for interpolating the unknown parameters of the transverse displacement component, the present finite element model almost satisfies the general requirements of compatibility and completeness. Thus, the introduced finite

Table 3 Static bending test results: simply supported FGM plate under transverse bi-sinosodial load

Plate model	n	$\bar{u}$	$\bar{v}$	$\bar{w}$	$\bar{\sigma}_{xx}$	$\bar{\sigma}_{yy}$	$\bar{\sigma}_{yz}$	$\bar{\sigma}_{xz}$	$\bar{\sigma}_{xy}$	$\bar{\sigma}_{zz}$	no. unknowns
Present	1	0.6480	0.5064	0.5831	3.1291	1.6063	0.2601	0.2503	0.6045	1.0000	6
Zenkour (2006)		0.6626	0.5093	0.5889	3.0870	1.4894	0.2622	0.2462	0.6110	-	5
Brischetto and Carrera (2010) (PVD)		0.6435	0.4981	0.5875	-	-	0.2510	-	-	0.9842	15
Brischetto and Carrera (2010) (RMVT)		0.6435	0.4980	0.5875	-	-	0.2510	-	-	0.9881	30
CLT (Neves *et al.* 2011)		-	-	0.5623	-	2.0150	-	-	-	-	3
FSDT (Neves *et al.* 2011)		-	-	0.5889	-	2.0150	-	-	-	-	5
Neves *et al.* (2011)		-	-	0.5845	-	1.4945	-	-	-	-	9
Present	2	0.9273	0.7413	0.7485	3.6243	1.4419	0.2396	0.2022	0.5295	1.0000	6
Zenkour (2006)		0.9281	0.7311	0.7573	3.6094	1.3954	0.2763	0.2265	0.5441		5
Brischetto and Carrera (2010) (PVD)		0.9012	0.7162	0.7570	-	-	0.2516	-	-	0.9309	15
Brischetto and Carrera (2010) (RMVT)		0.9012	0.7161	0.7570	-	-	0.2497	-	-	0.9610	30
CLT (Neves *et al.* 2011)		-	-	-	-	-	-	-	-	-	3
FSDT (Neves *et al.* 2011)		-	-	-	-	-	-	-	-	-	5
Neves *et al.* (2011)		-	-	-	-	-	-	-	-	-	9
Present	3	1.0104	0.8138	0.8279	4.1995	1.3797	0.2665	0.2136	0.5392	1.0000	6
Zenkour (2006)		1.0447	0.8271	0.8377	3.8742	1.2748	0.2715	0.2107	0.5525	-	5
Brischetto and Carrera (2010) (PVD)		1.0111	0.8086	0.8381	-	-	-	-	-	-	15
Brischetto and Carrera (2010) (RMVT)		1.0111	0.8086	0.8381	-	-	-	-	-	-	30
CLT (Neves *et al.* 2011)		-	-	-	-	-	-	-	-	-	3
FSDT (Neves *et al.* 2011)		-	-	-	-	-	-	-	-	-	5
Neves *et al.* (2011)		-	-	-	-	-	-	-	-	-	9
Present	4	1.0655	0.8521	0.8731	4.1011	1.2275	0.2304	0.1867	0.5501	1.0000	6
Zenkour (2006)		1.0941	0.8651	0.8819	4.0693	1.1783	0.2580	0.2029	0.5667	-	5
Brischetto and Carrera (2010) (PVD)		1.0548	0.8430	0.8822	-	-	-	-	-	-	15
Brischetto and Carrera (2010) (RMVT)		1.0549	0.8430	0.8822	-	-	-	-	-	-	30
CLT (Neves *et al.* 2011)		-	-	0.8281	-	1.6049	-	-	-	-	3
FSDT (Neves *et al.* 2011)		-	-	0.8736	-	1.6049	-	-	-	-	5
Neves *et al.* (2011)		-	-	0.8750	-	1.1783	-	-	-	-	9
Present	9	1.1144	0.8767	0.9848	5.0336	0.9582	0.1966	0.2113	0.5682	1.0000	6
Zenkour (2006)		1.1358	0.8785	0.9925	4.9303	0.9092	0.2072	0.2164	0.5875	-	5
Brischetto and Carrera (2010) (PVD)		-	-	-	-	0.9286	0.2107	-	0.5903	0.7277	15
Brischetto and Carrera (2010) (RMVT)		-	-	-	-	0.9285	0.2298	-	0.5905	1.0295	30
CLT (Neves *et al.* 2011)		-	-	-	-	-	-	-	-	-	3
FSDT (Neves *et al.* 2011)		-	-	-	-	-	-	-	-	-	5
Neves *et al.* (2011)		-	-	-	-	-	-	-	-	-	9
Present	10	1.1233	0.8623	1.0009	5.1410	0.9455	0.2032	0.2262	0.5730	1.0000	6
Zenkour (2006)		1.1372	0.8756	1.0089	5.0890	0.8775	0.2041	0.2198	0.5894	-	5
Brischetto and Carrera (2010) (PVD)		-	-	-	-	0.8966	0.2108	-	0.5925	0.7506	15
Brischetto and Carrera (2010) (RMVT)		-	-	-	-	0.8964	0.2289	-	0.5926	1.0580	30
CLT (Neves *et al.* 2011)		-	-	0.9354	-	1.1990	-	-	-	-	3
FSDT (Neves *et al.* 2011)		-	-	0.9966	-	1.1990	-	-	-	-	5
Neves *et al.* (2011)		-	-	0.8750	-	1.1783	-	-	-	-	9

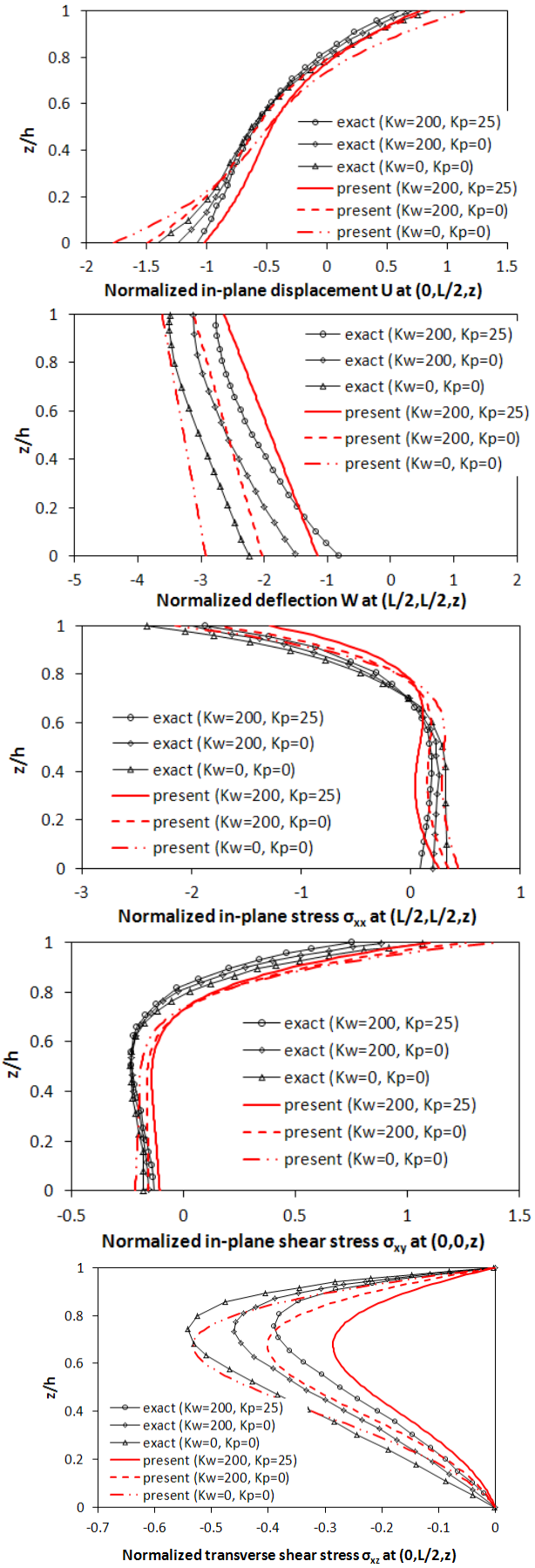

Fig. 3 Variations of the displacement and stress components along the thickness direction of the very thick FGM plate

element model does not show sensitivity versus the mesh distortion. Note that the term "completeness" means that the elements must have enough global basis functions to capture the analytical solution in the limit of a mesh distortion process. The term "compatibility" means that the shape functions should provide displacement continuity between elements to avoid the appearance of material gaps as the elements deform. As the mesh is refined, such gaps would multiply and may absorb or release spurious energy (Lee and Bathe 1993, Prathap *et al*. 2006).

4.1.3 Static bending analysis

The considered simply supported square FGM plate has been analyzed using the present partial mixed finite element model for different values of the material gradient indexes. Results are given in Table 3 in terms of displacement and stress components. In this table, the present results are compared with the results of the generalized shear deformation theory of Zenkour (2006), unified formulation of Brischetto and Carrera (2010) based on PVD and RMVT, sinusoidal plate formulation of Neves *et al.* (2011), and CLT and FSDT solutions. It can be observed that the results of the present partial mixed finite element model are in good agreement with other non-classical high-order plate theories. In the prediction of in-plane displacements of the FGM plate, the results of the classical (CLT and FSDT) and non-classical (present, Zenkour, Brischetto and Carrera, and Neves *et al*.) plate theories are very close together whatever the values of material gradient index n. Concerning the transverse displacement, the results of Neves *et al.* and CLT diverge from the results of other plate theories with increasing of n. It can be also seen from Table 3 that there exists a relatively high discrepancies between the axial stresses predicted by the classical plate theories and those predicted by the non-classical plate theories. This demonstrates that the classical plate theories are not sufficient for accurate analysis of FGM plates. Concerning the transverse shear stresses, differences exist between the present and the RMVT results. This shows that the only modeling of transverse normal stress (partial mixed model) may be not sufficient for the accurate analysis of the FGM plates in some cases. In order to have a comparison between the computational efficiency of these different plate models, the number of unknown parameters of each plate model is also given in Table 3. The computational efficiency of the present partial mixed finite element model can be easily inferred from this table. As stated previously in section 3.1, the present partial mixed kinematic has six unknown parameters. The employed quadrilateral element has 21 dofs per node. The finite element results of Table 3 are obtained using a mesh with 8×8 elements (1701 dofs).

4.2 Example 2

In this example, a very thick square ($a=b=L$) FGM plate rested on two-parameter elastic foundation has been analyzed using the present partial mixed finite element model. The Young's modulus of the considered plate varies exponentially along the thickness direction according to the following relation

$E(z)=\tilde{E}\,e^{n(1/2+z/h)}$

where $\tilde{E}$ denotes the value of elastic modulus at the bottom surface of the plate. The values of the material gradient index is taken as $n=\ln(10)$ and the Poisson's ratio is assumed to be $\nu=0.3$. The thickness ratio of the graded plate is *h/L*=0.5 and a transverse bi-sinusoidal load with the amplitude $q_0=\tilde{E}/10^5$ is applied on its top surface.

Through-the-thickness variations of the displacement and stress components of the FGM plate are depicted in Fig. 3 for different values of the foundation parameters. In these figures, the elastic foundation parameters are represented in the following non-dimensional forms

$K_w=k_w a^4/D$, $\qquad K_p=k_p a^2/D$

where $D=\tilde{E}h^3/12(1-\nu^2)$. The following non-dimensional forms are also used for the displacement and stress components

$\tilde{w}=10^6 w(L/2,L/2,z)/h$, $\tilde{u}=10^6 u(0,L/2,z)/h$

$\tilde{\sigma}_{xx}=\sigma_{xx}(L/2,L/2,z)/q_0$, $\tilde{\sigma}_{xy}=\sigma_{xy}(0,0,z)/q_0$

$\tilde{\sigma}_{xz}=\sigma_{xz}(0,L/2,0)/q_0$

In Fig. 3, the results of the present partial mixed finite element model have been compared with the exact 3D elasticity solutions of Huang *et al.* (2008). Note that the transverse shear component of the stress tensor ($\tilde{\sigma}_{xz}$) is calculated directly from the constitutive relations. Although the considered graded plate of the present example is strongly thick, the results of the present model are in relatively good agreement with the elasticity solutions. These results prove the accuracy of the present partial mixed finite element model for the static bending analysis of thick FGM plates.

It can be observed from Fig. 3 that all displacement and stress components of the FGM plate decrease gradually as either K_w or K_p increases. These decreases of stresses and displacements show that with increasing the foundation stiffness the rigidity of the plate is certainly enhanced. It is also seen from Fig. 3 that the variations of the transverse displacement (*W*) are not constant across the thickness as usually assumed in most of plate theories. Thanks to employing a linear distribution for the transverse deflection, the present finite element model can capture the non-constant variations of deflections in FGM plates with enough accuracy.

4.3 Example 3

Free vibration of a simply supported square FGM plate with thickness ratio *a/h*=5 is studied in this example. The Young's modulus and the density of the considered plate vary along the thickness direction as:

$E(z)=E_m\,e^{n(1/2+z/h)}$, $\qquad \rho(z)=\rho_m\,e^{n(1/2+z/h)}$

where $E_m=70GPa$ and $\rho_m=2702\,kg/m^3$. The Poisson's ratio is assumed to be *v*=0.3 and the value of the material gradient index is taken as *n*=2.3. In presenting the numerical results of this example, the following non-dimensional parameters are used

$\bar{\omega}=\dfrac{\omega a^2}{h}\sqrt{\rho_m/E_m}$, $\quad K_w=\dfrac{k_w a^4}{D_m}$,

$K_p=\dfrac{k_p a^2}{D_m}$, $\qquad D_m=\dfrac{E_m h^3}{12(1-\nu^2)}$

The predicted non-dimensional fundamental frequencies of the FGM plate are given in Table 4 for different values of the foundation parameters K_w, K_p. In this table, the results of the present partial mixed finite element model have been compared with exact 3D solutions of Lu *et al*. (2009) as well as the results of the refined shear deformation theory of Thai and Choi (2012). It is worth to note here that the plate model of Thai and Choi has four unknown parameters. It can be seen from Table 4 that the accuracy of the present partial mixed finite element model in the prediction of the fundamental frequencies of the FGM plate is much more than the refined plate model of Thai and Choi (2012). For different values of the foundation parameters, the maximum error of the present model in the prediction of the fundamental frequency is 2.08%. This value for the refined model of Thai and Choi is 7.66%. The lower accuracy of the refined plate model of Thai and Choi (2012) in the prediction of the natural frequencies may be attributed to the neglecting of the thickness stretching effects.

4.4 Example 4

Free vibration of an FGM plate with SSSC boundary conditions and the thickness ratio *a/h*=10 is carried out in this section. SSSC indicates that the graded plate is clamped at *y*=*b* and the other edges are simply supported. The mechanical properties of the plate are as follows

$E(z)=E_m+(E_c-E_m)\left(\dfrac{1}{2}+\dfrac{z}{h}\right)^n$

$\rho(z)=\rho_m+(\rho_c-\rho_m)\left(\dfrac{1}{2}+\dfrac{z}{h}\right)^n$, $\qquad \nu=0.3$

where $E_c=380GPa$, $E_m=70GPa$, $\rho_c=3800\,kg/m^3$ and $\rho_m=2702\,kg/m^3$. The nondimensional fundamental frequencies of the graded plate predicted by the present partial mixed finite element model are given in Table 5 for different values of the foundation parameters, aspect ratios *a/b* and material gradient index *n*. Note that the definitions of the non-dimensional parameters are similar to the previous example. In Table 5, the results of the refined shear deformation theory of Thai and Choi (2012) are also shown. Similar to the previous example, it is seen that the present results are in good agreement with those generated by Thai and Choi (2012).

It can be noticed from Table 5 that with increasing of Winkler and Pasternak foundation parameters, natural frequency of vibration increases. As it can be seen, Pasternak parameter has more effect on increasing the natural frequency than the Winkler parameter. By comparing the numerical results cited in Tables 4 and 5, it can also be concluded that the effect of Pasternak foundation on increasing the natural frequency in FGM

Table 4 Non-dimensional fundamental frequency of the simply supported square FGM plate

K_w	K_p	a/h=5, n=2.3				
		Exact (Lu *et al.* 2009)	Thai and Choi (2012)	Error (%)	Present	Error (%)
0	0	4.7524	5.1163	7.66	4.8267	1.56
	10	5.1964	5.5300	6.42	5.2370	0.78
	25	5.7978	6.0982	5.18	5.7918	0.10
10	0	4.7759	5.1381	7.58	4.8484	1.51
	10	5.2179	5.5502	6.37	5.2568	0.74
	25	5.8170	6.1164	5.15	5.8094	0.13
100	0	4.9824	5.3299	6.97	5.0389	1.13
	10	5.4072	5.7282	5.94	5.4313	0.44
	25	5.9870	6.2784	4.87	5.9655	0.35
1000	0	6.6999	6.9634	3.93	6.6158	1.25
	10	7.0192	7.2728	3.61	6.9066	1.50
	25	7.4716	7.7136	3.24	7.3161	2.08

Table 5 Non-dimensional fundamental frequency of the SSSC graded plate

K_w	K_p	a/b	n=0		n=1		n=5		n=10	
			Present	Thai and Choi (2012)	Present	Thai and Choi (2012)	Present	Thai and Choi (2012)	Present	Thai and Choi (2012)
0	0	0.5	7.4840	7.5013	5.7524	5.7399	4.9253	4.9111	4.7477	4.7446
	100		11.6571	11.7074	11.2004	11.2760	11.2904	11.3993	10.7872	11.4676
100	0		7.9031	7.9195	6.3698	6.3622	5.7154	5.7092	5.5874	5.5898
	100		11.9302	11.9796	11.5288	11.6051	11.6546	11.7651	10.7873	11.8423
0	0	1	13.4201	13.4339	10.3547	10.3056	8.7994	8.7548	8.4596	8.4376
	100		17.6855	17.7236	16.1059	16.1763	15.6925	15.8249	15.6708	15.8113
100	0		13.6570	13.6706	10.7065	10.6626	9.2599	9.2234	8.9535	8.9375
	100		17.8656	17.9036	16.3335	16.4061	15.9529	16.0889	15.9401	16.0837
0	0	2	39.6899	36.1015	30.6331	27.9647	26.0886	23.1627	25.0853	22.1316
	100		43.8958	40.5304	36.6639	34.3067	33.6498	31.2410	33.0800	30.6913
100	0		39.7710	36.1890	30.7549	28.0960	26.2491	23.3411	25.2576	22.3246
	100		43.9692	40.6084	36.7657	34.4138	33.7742	31.3735	33.2107	30.8307

Table 6 Non-dimensional fundamental frequency of the SCSC graded plate (h/a=0.2)

K_w	K_p	n=0		n=0.5		n=1		n=2		n=10	
		Present	Baferani *et al.* (2011)	Present	Baferani *et al.* (2011)	Present	Baferani *et al.* (2011)	Present	Baferani *et al.* (2011)	Present	Baferani *et al.* (2011)
0	0	0.5586	0.5363	0.4836	0.4680	0.4397	0.4263	0.3967	0.3844	0.3566	0.3447
	100	0.7187	0.7033	0.6714	0.6725	0.6450	0.6556	0.5903	0.6421	0.5100	0.6308
100	0	0.5675	0.5457	0.4947	0.4799	0.4524	0.4402	0.4114	0.4007	0.3740	0.3639
	100	0.7255	0.7105	0.6791	0.6809	0.6531	0.6647	0.5903	0.6521	0.5100	0.6416

plates with SSSC boundary conditions is more significant than those with SSSS boundary conditions.

4.5 Example 5

Free vibration of the FGM plates with various boundary conditions are investigated in this example. The material properties of the considered FGM plates of the present example as well as the definitions of the non-dimensional foundation parameters are similar to the previous example. The considered FGM plates have square shape and their thickness ratio is taken as h/a=0.2. In Tables 6-7, the fundamental non-dimensional frequencies ($\hat{\omega} = \omega h \sqrt{\rho_m / E_m}$) of the graded plates with SCSC and SCSF boundary conditions are compared with those given by Baferani *et al*. (2011) based on the TSDT. It can be seen that the results of the present partial mixed finite element model coincide with those of TSDT for different values of the foundation parameters and material gradient indexes. It is worthy to note that the number of unknown parameters of the plate model of Baferani *et al*. (2011) is the same as the present partial mixed plate model. However, the present mixed plate model takes into account the thickness stretching effects. These numerical results again prove the accuracy of the proposed mixed finite element model for the free vibration analysis of the FGM plates rested on elastic foundations.

Table 7 Non-dimensional fundamental frequency of the SCSF graded plate (h/a=0.2)

K_w	K_p	n=0		n=0.5		n=1		n=2		n=10	
		Present	Baferani *et al.* (2011)	Present	Baferani *et al.* (2011)	Present	Baferani *et al.* (2011)	Present	Baferani *et al.* (2011)	Present	Baferani *et al.* (2011)
0	0	0.2773	0.2714	0.2369	0.2338	0.2139	0.2121	0.1937	0.1925	0.1797	0.1781
	100	0.4539	0.4531	0.4420	0.4491	0.4358	0.4481	0.4319	0.4499	0.4327	0.4552
100	0	0.2948	0.2894	0.2590	0.2570	0.2393	0.2389	0.2227	0.2235	0.2125	0.2132
	100	0.4647	0.4641	0.4539	0.4616	0.4483	0.4615	0.4447	0.4642	0.4459	0.4707

From Tables 6-7, it can be observed that for SCSC and SSSC boundary conditions, the natural frequencies decrease with the increase of power law index. Similar to section 4.4, it is seen again that the Pasternak elastic foundation has more significant effect in increasing the natural frequency of the FGM plate.

5. Conclusions

A computationally efficient partial mixed finite element model was introduced for the static and free vibration analyses of FGM plates rested on Winkler-Pasternak elastic foundations. The mechanical properties of the plate are assumed to vary continuously along the thickness direction according to simple exponent/power-law distributions. The proposed finite element model, which is based on a parametrized mixed variational principle, has only one general unknown function more than FSDT. It can predict through-the-thickness variations of the transverse shear and normal stresses directly from the constitutive equation. The boundary conditions of the shear and normal stresses on the top and bottom surfaces of the FGM plates are also satisfied. The in-plane variations of the transverse deflection are interpolated using full Hermitian shape functions while C^0-type continuity is considered for in-plane variations of other unknown parameters of the stress

and displacement fields. The convergence velocity of the proposed finite element model is high and it is not sensitive to the mesh distortion. The numerical studies show that the present finite element model gives accurate results for thick-to-thin FGM plates with different material gradient indexes and various boundary and loading conditions.

Future researches are pointed towards the extension of the present finite element formulation to geometrically and materially nonlinear analysis of laminated composite and sandwich plates/shells.

References

Akavci, S.S. (2014), "An efficient shear deformation theory for free vibration of functionally graded thick rectangular plates on elastic foundation", *Compos. Struct.*, **108**, 667-676.

Batra, R.C. (2007), "Higher-order shear and normal deformable theory for functionally graded incompressible linear elastic plates", *Thin-Wall. Struct.*, **45**(12), 974-982.

Brischetto, S. and Carrera, E. (2010), "Advanced mixed theories for bending analysis of functionally graded plates", *Comput. Struct.*, **88**(23-24), 1474-1483.

Buczkowski, R. and Torbacki, W. (2001), "Finite element modelling of thick plates on two-parameter elastic foundation", *Int. J. Numer. Anal. Meth. Geomech.*, **25**(14), 1409-1427.

Hadji, L., Ait Amar Meziane, M., Abdelhak, Z., Hassaine Daouadji, T. and Adda Bedia, E.A. (2016), "Static and dynamic behavior of fgm plate using a new first shear deformation plate theory", *Struct. Eng. Mech.*, **57**(1), 127-140.

Hasani Baferani, A., Saidi, A.R. and Ehteshami, H. (2011), "Accurate solution for free vibration analysis of functionally graded thick rectangular plates resting on elastic foundation", *Compos. Struct.*, **93**(7), 1842-1853.

Hassaine Daouadji, T. and Adim, B. (2017), "Mechanical behaviour of fgm sandwich plates using a quasi-3D higher order shear and normal deformation theory", *Struct. Eng. Mech.*, **61**(1), 49-63.

Huang, Z.Y., Lu, C.F. and Chen, W.Q. (2008), "Benchmark solutions for functionally graded thick plates resting on Winkler–Pasternak elastic foundations", *Compos. Struct.*, **85**(2), 95-104.

Kitipornchai, S., Yang, J. and Liew, K.M. (2006), "Random vibration of the functionally graded laminates in thermal environments", *Comput. Meth. Appl. Mech. Eng.*, **195**(9-12), 1075-1095.

Lee, N.S. and Bathe, K.J. (1993), "Effects of element distortions on the performance of isoparametric elements", *Int. J. Numer. Meth. Eng.*, **36**(20), 3553-3576.

Lezgy-Nazargah, M. (2015a), "A three-dimensional exact state-space solution for cylindrical bending of continuously non-homogenous piezoelectric laminated plates with arbitrary gradient composition", *Arch. Mech.*, **67**(1), 25-51.

Lezgy-Nazargah, M. (2015b), "Fully coupled thermo-mechanical analysis of bi-directional FGM beams using NURBS isogeometric finite element approach", *Aerosp. Sci. Technol.*, **45**, 154-164.

Lezgy-Nazargah, M. (2016a), "A three-dimensional Peano series solution for the vibration of functionally graded piezoelectric laminates in cylindrical bending", *Sci. Iranic. A*, **23**(3), 788-801.

Lezgy-Nazargah, M. (2016b), "A high-performance parametrized mixed finite element model for bending and vibration analyses of thick plates", *Acta Mech.*, **227**(12), 3429-3450.

Lezgy-Nazargah, M. and Cheraghi, N. (2017), "An exact Peano Series solution for bending analysis of imperfect layered FG neutral magneto-electro-elastic plates resting on elastic foundations", *Mech. Adv. Mater. Struct.*, **24**(3), 183-199.

Lu, C.F., Lim, C.W. and Chen, W.Q. (2009), "Exact solutions for free vibrations of functionally graded thick plates on elastic foundations", *Mech. Adv. Mater. Struct.*, **16**(8), 576-584.

Malekzadeh, P. (2009), "Three-dimensional free vibration analysis of thick functionally graded plates on elastic foundations", *Compos. Struct.*, **89**(3), 367-373.

Mantari, J.L. and Guedes Soares, C. (2014), "A trigonometric plate theory with 5-unknowns and stretching effect for advanced composite plates", *Compos. Struct.*, **107**, 396-405.

Mantari, J.L., Bonilla, E.M. and Guedes Soares, C. (2014), "A new tangential-exponential higher order shear deformation theory for advanced composite plates", *Compos. Part B*, **60**, 319-328.

Matsunaga, H. (2008), "Free vibration and stability of functionally graded plates according to a 2-D higher-order deformation theory", *Compos. Struct.*, **82**(4), 499-512.

Neves, A.M.A., Ferreira, A.J.M., Carrera, E., Roque, C.M.C., Cinefra, M., Jorge, R.M.N. and Soares, C.M.M. (2011), "Bending of FGM plates by a sinusoidal plate formulation and collocation with radial basis functions", *Mech. Res. Commun.*, **38**(5), 368-371.

Prathap, G., Senthilkumar, V. and Manju, S. (2006) "Mesh distortion immunity of finite elements and the best-fit paradigm" *Sadhan.*, **31**(5), 505-514.

Shaban, M. and Alipour, M.M. (2011), "Semi-analytical solution for free vibration of thick functionally graded plates rested on elastic foundation with elastically restrained edge", *Acta Mech. Sol. Sin.*, **24**(4), 340-354.

Sheikholeslami, S.A. and Saidi, A.R. (2013), "Vibration analysis of functionally graded rectangular plates resting on elastic foundation using higher-order shear and normal deformable plate theory", *Compos. Struct.*, **106**, 350-361.

Sobhy, M. (2013), "Buckling and free vibration of exponentially graded sandwich plates resting on elastic foundations under various boundary conditions", *Compos. Struct.*, **99**, 76-87.

Thai, H.T. and Choi, D.H. (2012), "A refined shear deformation theory for free vibration of functionally graded plates on elastic foundation", *Compos. Part B*, **43**(5), 2335-2347.

Yang, J., Liew, K.M. and Kitipornchai, S. (2005), "Stochastic analysis of compositionally graded plates with system randomness under static loading", *Int. J. Mech. Sci.*, **47**(10), 1519-1541.

Yas, M.H. and Sobhani Aragh, B. (2010), "Free vibration analysis of continuous grading fiber reinforced plates on elastic foundation", *Int. J. Eng. Sci.*, **48**(12), 1881-1895.

Zenkour, M.A. (2006), "Generalized shear deformation theory for bending analysis of functionally graded plates", *Appl. Math. Modell.*, **30**(1), 67-84.

CC

Appendix A

$$\boldsymbol{D}_{pp}=\begin{bmatrix} \frac{E(z)}{(1-\nu^2)} & \frac{\nu E(z)}{(1-\nu^2)} & 0 & 0 & 0 \\ \frac{\nu E(z)}{(1-\nu^2)} & \frac{E(z)}{(1-\nu^2)} & 0 & 0 & 0 \\ 0 & 0 & \frac{E(z)}{2(1+\nu)} & 0 & 0 \\ 0 & 0 & 0 & \frac{E(z)}{2(1+\nu)} & 0 \\ 0 & 0 & 0 & 0 & \frac{E(z)}{2(1+\nu)} \end{bmatrix}$$

$$\boldsymbol{D}_{pz}^{T}=\begin{bmatrix} \frac{\nu E(z)}{(1-\nu^2)} & \frac{\nu E(z)}{(1-\nu^2)} & 0 & 0 & 0 \end{bmatrix},$$

$$\boldsymbol{D}_{zz}=\begin{bmatrix} \frac{E(z)}{(1-\nu^2)} \end{bmatrix}$$

$$L_1=\frac{2}{h^2}z\,(z-\frac{h}{2}),\quad L_2=\frac{4}{h^2}(\frac{h}{2}+z)(\frac{h}{2}-z),$$

$$L_3=\frac{2}{h^2}z\,(z+\frac{h}{2})$$